Electronic Supplement to

A new strategy to compare inverted rupture models exploiting the eigen-structure of the inverse problem

by František Gallovič and Jean-Paul Ampuero

The Electronic Supplement contains appendix explaining the conversion of inverted models from the SIV database (model SIV2a) to a unified spatial-temporal discretization, table with description of the inverted models, and figures showing all the inverted models in full spectrum and after SVD truncation.

Conversion of inverted models to a unified discretization

The fault plane in the SIV2a benchmark is 40 km x 20 km large. The integral in the representation theorem is discretized assuming 1.5 km x 1.0 km large subfaults and 0.4 s time step. The displacement Green's functions are Butterworth filtered (one way, 4 poles, bandpass 0.05-0.5 Hz). These settings follow recommended relations between space-time sampling and frequency to guarantee sufficient accuracy (e.g., Spudich and Archuleta, 1987; Beresnev, 2003). The spectrum of the matrix G is shown in Figure 1c.

Models Gallovic0.01 and Gallovic0.1 were obtained assuming the above-mentioned discretization. The other models considered (Target, Hoby, CedricT3, Asano) were resampled to the common discretization according to the following procedure:

- Rupture times, rise times and slip values are bilinearly interpolated onto a grid 10 times denser than the common one (150 m x 100 m) and temporally interpolated at 10 times higher sampling rate (0.04 s).
- The slip rates evaluated on the dense grid are smoothed by a running mean over 10 x 10 samples in space and 10 samples in time.
- The slip rates are then downsampled to 1.5 km x 1.0 km and 0.4 s.

This procedure captures correctly the shape of the slip rate functions considered by the authors, i.e. it minimizes aliasing effects that could be significant especially when dealing with sharp triangular slip rates considered in some of the methods (see Table S1).

Table

Model name *Method*	Description	Data processing
Gallovic0.01 *Gallovič et al. (2015)*	Linear multi-time window inversion approach with long duration of slip rate functions (equal to the assumed duration of the rupture process). Constraints: i) smoothing by means of a prior k^{-2} covariance functions, ii) positivity of the slip rate function. The smoothing weight is relatively small (perhaps not applicable in real-data application).	Bandpass Butterworth filter in range of 0.05-0.5 Hz (4 poles, causal).
Gallovic0.1 *Gallovič et al. (2015)*	Same as Gallovic0.01, but with more severe smoothing (similar to that used in real data applications).	Same as Gallovic0.01.
Hoby *Razafindrakoto et al. (2014)*	Parametric (single-time window) inversion assuming triangular slip rate function. Parameters: rupture times, rise times, peak slip rates. Metropolis algorithm is used to optimize the parameters considering L2-norm.	Butterworth bandpass in range of 0.01-1 Hz.
CedricT3 *Twardzik et al. (2012)*	Simplified source model considering two elliptical subfault patches, triangular slip rate function and constant rupture velocities along the patches. Parameters: location and size of the ellipses, rupture velocities, onset times of the subfault patches. Neighborhood algorithm is used to find the best fitting parameters considering L2-norm.	Butterworth bandpass filter in range of 0.1 - 1.0 Hz (4 poles, 2 passes - acausal).
Asano *Sekiguchi et al. (2000)*	Multi-time window linear inversion with spatiotemporal smoothing constraint. Weight of smoothing is determined by minimizing ABIC.	Bandpass filter in range of 0.05 - 1.0 Hz.

Table S1: List of the inverted models of the SIV2a benchmark with brief explanation of the applied inversion techniques.

Figures

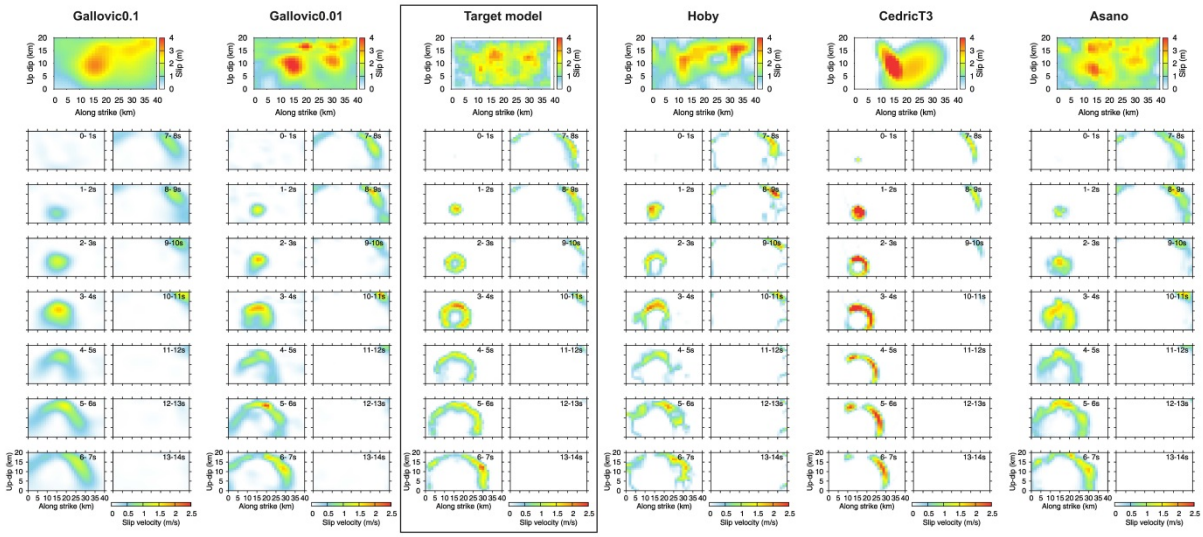

Figure S1: Inversion results of the SIV2a benchmark obtained by various authors (see Table S1): slip distributions (top-most panels) and slip rate snapshots (bottom panels). Stars in the slip plots denote locations for which slip rates are shown in Figure 4a.

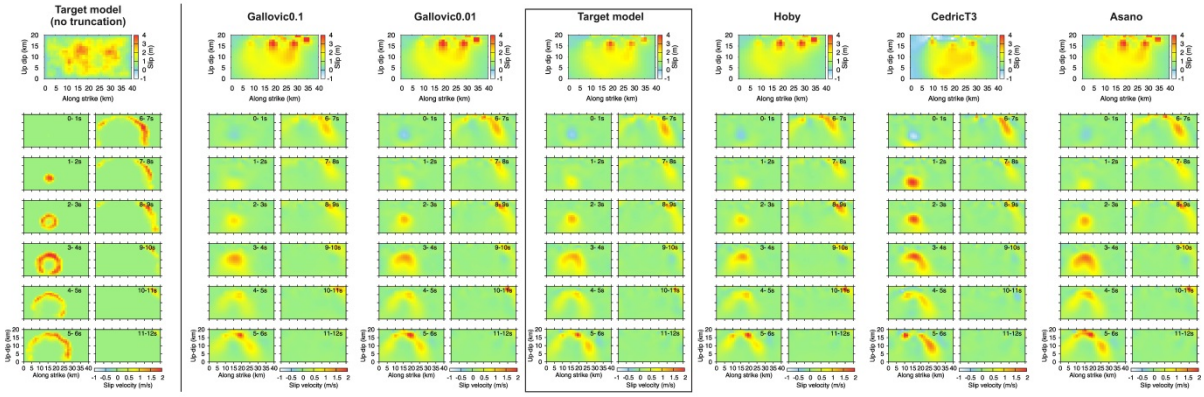

Figure S2: Target model and individual inversion results (columns) truncated with cut-off at 1/10 of the largest singular value: slip distributions (top-most panels) and slip rate snapshots (bottom panels). The original target model is shown on the left, for reference, in the same color scale.

References

Beresnev (2003). Uncertainties in Finite-Fault Slip Inversions: To What Extent to Believe? (A Critical Review), Bull. Seism. Soc. Am. 93, 2445-2458.

Gallovič, F., W. Imperatori, and P. M. Mai (2015). Effect of three-dimensional velocity heterogeneities and topography on slip inversions: case study of the Mw6.3 2009 L'Aquila earthquake, J. Geophys. Res. 120, 428-449.

Razafindrakoto, H. N. T., and M. P. Mai (2014). Uncertainty in Earthquake Source Imaging Due to Variations in Source Time Function and Earth Structure, Bull. Seismol. Soc. Am. 104, 855–874.

Sekiguchi, H., K. Irikura, and T. Iwata (2000), Fault geometry at the rupture termination of the 1995 Hyogo-ken Nanbu earthquake, Bull. Seism. Soc. Am. 90, 117-133.

Spudich, P., and R. J. Archuleta (1987). Techniques for Earthquake Ground-Motion Calculation with Applications to Source Parametrization of Finite Faults, in Seismic Strong Motion Synthetics, B. A. Bolt (Editor), Academic Press, Orlando, Florida, 205–265.

Twardzik, C., Madariaga, R., Das, S. and S. Custódio S. (2012). Robust features of the source process for the 2004 Parkfield, California, earthquake from strong-motion seismograms. Geophys. J. Int. 191, 1245-1254.